Nanoscale

PAPER

View Article Online
View Journal | View Issue

Cite this: *Nanoscale*, 2017, **9**, 8756

The impact of metalation on adsorption geometry, electronic level alignment and UV-stability of organic macrocycles on TiO_2(110)†

Manuel Graf, ‡[a] Gerson Mette, *§[a] Dominik Leuenberger,[a] Yeliz Gurdal,[b] Marcella Iannuzzi,[b] Wolf-Dietrich Zabka,[a] Stephan Schnidrig,[b] Benjamin Probst,[b] Jürg Hutter,[b] Roger Alberto[b] and Jürg Osterwalder *[a]

Received 1st April 2017,
Accepted 5th June 2017

DOI: 10.1039/c7nr02317k

rsc.li/nanoscale

Metal complexes of the tetradentate bipyridine based macrocycle pyrphyrin (Pyr) have recently shown promise as water reduction catalysts in homogeneous photochemical water splitting reactions. In this study, the adsorption and metalation of pyrphyrin on stoichiometric TiO_2(110) is investigated in ultrahigh vacuum by means of scanning tunneling microscopy, photoelectron spectroscopy, low-energy electron diffraction, and density functional theory. In a joint experimental and computational effort, the local adsorption geometry at low coverage, the long-range molecular ordering at higher coverage and the electronic structure have been determined for both the bare ligand and the cobalt-metalated Pyr molecule on TiO_2. The energy level alignment of CoPyr/TiO_2 supports electron injection into TiO_2 upon photoexcitation of the CoPyr complex and thus renders it a potential sensitizer dye. Importantly, Co-incorporation is found to stabilize the Pyr molecule against photo-induced degradation, while the bare ligand is decomposed rapidly under continuous UV-irradiation. This interesting phenomenon is discussed in terms of additional de-excitation channels for electronically highly excited molecular states.

1. Introduction

Splitting water into hydrogen and oxygen by means of solar light is a promising strategy towards an environmentally sustainable energy harvesting and storage solution.[1] Although the efficiency was modest, electrochemical photolysis of water at a TiO_2 semiconducting electrode was demonstrated already in 1972 by Fujishima *et al.*[2] Titania has since become the best studied material for photocatalytic hydrogen and oxygen evolution[3] and for heterogeneous photocatalysis in general.[4,5] Water can also be split in homogeneous reactions, and metal–organic complexes have revealed excellent photocatalytic properties.[6] Cobalt complexes in particular have received much attention for photocatalytic hydrogen production, including Co-porphyrin.[7] Recently, cobalt complexes with a purely pyridine-based macrocycle have shown to be robust and efficient water reduction catalysts.[8] Furthermore, these complexes feature excellent absorption properties with a potential use as photosensitizers. This macrocycle had been introduced first by Ogawa[9] and is termed pyrphyrin (Pyr) owing to its close relation to the porphyrins.

The combination of molecular and semiconductor catalysts with light absorbers offers great opportunities for optimizing the efficiency of solar water splitting. Charge transfer reactions in homogeneous systems are kinetically limited by the diffusion of electron relays and sacrificial donors, and they are therefore prone to short-circuiting recombination processes. By immobilizing molecular catalysts and/or photosensitizers on semiconductor surfaces, photoexcited charges can be separated on much faster time scales. This concept has been recently applied to an organic dye-sensitized tandem photoelectrochemical cell which can split water by solar light without applying any bias voltage.[10]

Photoinduced charge transfer processes at molecule–semiconductor interfaces are controlled by the alignment of molecular energy levels with respect to the valence and conduction band edges of the semiconductor at the surface, as well as by the electrostatic energy landscape defined by band bending

[a]*Physik-Institut, Universität Zürich, CH-8057 Zürich, Switzerland.*
E-mail: gerson.mette@physik.uni-marburg.de, osterwal@physik.uzh.ch;
Tel: +41 (0)44 635 5827
[b]*Institut für Chemie, Universität Zürich, CH-8057 Zürich, Switzerland*

† Electronic supplementary information (ESI) available: More details and results of the photoelectron spectroscopy experiments and the DFT calculations including also the coordinates of the calculated configurations. See DOI: 10.1039/C7NR02317K

‡ Present address: Empa, Swiss Federal Laboratories for Materials Science and Technology, CH-8600 Dübendorf, Switzerland.
§ Present address: Fachbereich Physik, Philipps-Universität Marburg, D-35037 Marburg, Germany.

and surface dipoles. The nature and the dynamics of these processes determine the catalytic activity of surface-attached molecules and their photostability. Surface science methods applied to molecular model catalysts on single crystalline surfaces can provide direct information on these properties. In this manuscript, we investigate the bonding geometry and the electronic structure of the molecular catalyst Co-pyrphyrin (CoPyr) immobilized on a rutile TiO_2(110) surface by means of scanning tunneling microscopy (STM), photoelectron spectroscopy (XPS/UPS), low-energy electron diffraction (LEED) and density functional theory (DFT). A recent DFT study of this system[11] showed that the electronic properties of the Co^{2+} center, which is the active center in the homogeneous case,[8] are not modified upon adsorption. Furthermore, the predicted energy level alignment indicates that CoPyr could potentially be used for efficient dye sensitization of TiO_2, since electron injection into the substrate upon absorption of visible light appears favorable. Our experimental study confirms both of these findings qualitatively, although minor deviations in the level alignment are observed.

Inspired by many adsorption and metalation studies of porphyrins and phthalocyanines,[12] we performed a comparative study of the unmetalated Pyr ligand and CoPyr adsorbed on TiO_2(110) in order to elucidate the role of the Co^{2+} center on the molecular levels and their alignment with respect to the substrate. Controlled *in situ* metalation of the Pyr molecules with cobalt is found to induce only minor changes in the valence band structure and does not affect the long-range molecular ordering. In contrast to a recently reported study of Pyr on Au(111),[13] the metalation reaction on TiO_2(110) proceeds readily at room temperature. Importantly, we observe that the incorporation of cobalt atoms into the Pyr molecules dramatically enhances their stability against UV-radiation. This increased photostability is assigned to additional de-excitation channels for electronically highly excited molecular states, due to an enhanced coupling between molecule and substrate, the variability of the Co oxidation state or additional soft vibrational modes introduced by Co-incorporation.

2. Experimental

We used monocrystalline rutile TiO_2(110) samples supplied by PI-KEM. Ar^+-sputtering (1 keV) and annealing (1100 K) rendered flat, near-stoichiometric (1 × 1) surfaces. The pyrphyrin molecules are vapor-deposited from a Knudsen cell at 579 K onto the sample held at room temperature. For metalation, cobalt is evaporated from a Co-tube of high purity permeated by a W-filament which is resistively heated. Preparation and deposition is accomplished under ultrahigh vacuum (UHV) conditions ($p \leq 5 \times 10^{-9}$ mbar); all measurements were performed *in situ* in a user-modified Vacuum Generators ESCALAB 220 ($p \leq 2 \times 10^{-10}$ mbar) as described in ref. 14. Core level and valence band spectra are recorded with MgKα ($h\nu$ = 1253.6 eV) and HeIα ($h\nu$ = 21.2 eV) radiation, respectively. The XPS binding energy scale is referenced to the O 1s position of TiO_2 at 530.4 eV (ref. 15) whereas for the UPS measurements the Fermi level was calibrated with a polycrystalline Ag sample, where an energy resolution of 125 meV was determined. For quantitative analysis of the molecular coverage and the metalation reaction, core-level spectra were deconvolved by symmetric Voigt functions after removal of a Shirley background. The STM measurements were conducted at room temperature in a Park Scientific VPII instrument attached to the same UHV system, using electrochemically etched W-tips.

Calculations are performed at the Kohn–Sham DFT level using a Gaussian and plane wave formalism as implemented in the CP2K/QUICKSTEP package.[16] Valence electrons are treated explicitly, while norm-conserving pseudo potentials[17] are used to describe the interactions between the valence electrons and the atomic cores. The valence shells contain 12, 6, 4, 1, and 5 electrons for Ti, O, C, H, and N, respectively. Double-zeta plus polarization basis sets, optimized on molecular geometries,[18] are adopted for all atomic types. A 600 Ry energy cutoff is used for the auxiliary plane wave expansion of the charge density. All geometry optimization runs are carried out using the Perdew–Burke–Enzerhof (PBE) exchange–correlation density functional[19] together with the Grimme–D3 dispersion interaction correction scheme.[20] Once optimized geometries are obtained, the Heyd–Scuseria–Ernzerhof (HSE06) hybrid density functional[21,22] is used for the electronic structure analysis. Indeed, HSE06 was shown to well reproduce the electronic structure characteristics of rutile TiO_2 [23] and porphyrin-based molecules.[24] All hybrid functional calculations are performed with the help of the auxiliary density matrix method (ADMM).[25–27] Further computational details are contained in the ESI.† In this work, we simulate the adsorption geometries and the electronic structures of the Pyr monomer as well as the Pyr and CoPyr monolayers, all on the rutile TiO_2(110) surface. For the calculations of the CoPyr monomer on TiO_2(110), we refer to our previous study.[11]

3. Results and discussion

Deposition of 0.1 monolayer (1 ML ≙ 1 Pyr molecule per 8 TiO_2 surface unit cells; based on LEED results below) of pyrphyrin on TiO_2(110) yields randomly distributed adsorbates without apparent preferential sites or clustering, as observable in the room temperature STM images of Fig. 1. Individual Pyr molecules appear rather blurred on the TiO_2(110) surface, much more so than in a recent study of Pyr adsorption on Au(111) where a distinct donut shape was imaged.[13] Nevertheless, submolecular structure is seen also on TiO_2(110) in the form of two lobes. At closer inspection, these lobes are aligned along two directions A and B indicated by green and blue lines in Fig. 1d. The same figure shows faint dark rows highlighted by white lines. These dark rows, shown with enhanced contrast in Fig. 1b, correspond to the salient bridging-oxygen rows along the [001]-direction of the TiO_2(110) surface.[29] They provide an excellent reference for determining the adsorption sites and orientations of the adsorbates: the

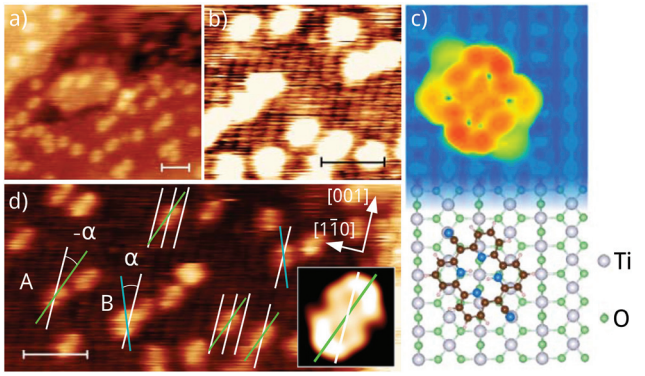

Fig. 1 Empty state STM images of 0.1 ML Pyr on TiO_2(110). (a) Adsorbed Pyr molecules appear as bright elliptical configurations. (b) Region of (d) with optimized contrast for the dark lines representing the bridging-oxygen rows of the substrate. (c) Calculated adsorption geometry with the minimal total energy (bottom) and the corresponding simulated STM image at a virtual sample bias U_s = 2.4 V (top). (d) Submolecular resolution exhibits two lobes per molecule which allow to identify the molecular orientation with respect to the bridging-oxygen rows (highlighted by white lines). Two molecular orientations A and B indicated with green and blue lines, respectively, are observed with the molecular axis rotated by $\alpha \approx \pm 19°$ with respect to [001]. The inset of (d) represents the calculated STM image from (c) which was blurred for better comparability. Note that images (b) and (d) were corrected for a linear drift[28] (tunneling conditions: U_s = 2.4 V, I_t = 151 pA, scale bar ≙ 3 nm).

bridging-oxygen rows all intersect the molecules at the center between the two lobes. The two orientations A and B show up with respective angles of −18 ± 6° and 20 ± 3° relative to the [001]-direction. A statistical evaluation of 160 molecules reveals a ratio of A : B = 1 : 1.1, suggesting that A and B are symmetrically equivalent orientations with the bridging-oxygen row forming the mirror axis.

Given the blurriness of the STM data, the absolute orientation of the molecules cannot be identified unambiguously without resorting to DFT calculations. The bottom part of Fig. 1c shows the optimized monomer adsorption geometry, in which the Pyr molecule straddles one of the oxygen rows with its cyano axis slightly rotated with respect to it. Please note, that in this molecular geometry two adsorption configurations with the two protons attached to different pyridinic nitrogen atoms are possible (*cf.* Fig. S7 and S8 in ESI†). However, both configurations exhibit almost the same adsorption energy and structure. In both configurations, the molecule is slightly bent along the cyano axis in a convex fashion due to the bonding of the two cyano end groups to surface Ti atoms. Hence, as shown in the upper part of Fig. 1c, the combination of elevation above the oxygen row and enhanced electron density at the pyridine rings finally leads to a pronounced elliptic structure in the calculated STM image. For better comparability with the experimental STM data, the inset in Fig. 1d presents this calculation at reduced resolution, obtained by Gaussian blurring. The two-lobe submolecular structure is well reproduced, and, accordingly, the white line indicates the [001]-direction while the green line links the two lobes. The resulting angle between the two lines in the inset is 20 ± 5° and thus consistent with the measured rotation angles. The STM images therefore provide confidence in the adsorption geometry derived from DFT.

The *in situ* metalation of Pyr/TiO_2(110) with cobalt is studied by means of core level spectroscopy. The N 1s spectrum of 1 ML of pyrphyrin in Fig. 2a shows two peaks. Apart from a weak shake-up satellite (dashed lines in Fig. 2a–c) which is common for such delocalized systems,[30] the spectrum can be well fitted by three peaks of equal intensity according to the three different nitrogen species present in the pyrphyrin molecule. The peaks at binding energies of 401.0 eV, 399.4 eV and 398.9 eV are assigned to pyridinic (N–H), cyano (C≡N) and iminic (C=N) nitrogen following the results obtained for Pyr/Au(111).[13] Subsequent deposition of a stoichiometric amount of cobalt leads to the incorporation of metal ions in the center of the molecules according to the reaction: Co(0) + Pyr → Co(II)Pyr + H_2. The increased oxidation state of bound Co can be observed by a shift of 1.9 eV towards higher binding energy in the Co 2p spectrum (*cf.* Fig. S1 in ESI†). Whereas the cyano groups are unaffected by the metalation, the nitrogen atoms of the molecular core are rendered equivalent by the incorporation of four-fold coordinated Co and the release of molecular hydrogen. This manifests itself in the appearance of

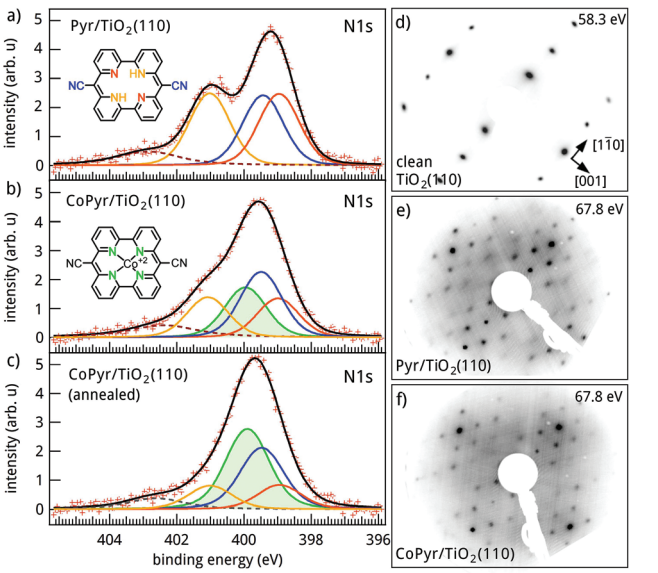

Fig. 2 (a) Core-level spectroscopy of the N 1s state from 1 ML Pyr on TiO_2(110). The spectrum can be fitted by three main peaks representing the three different species of nitrogen atoms in the structure formula of pyrphyrin (inset): the pyridinic-N (401.0 eV, orange), the cyano-N (399.4 eV, blue), and the iminic-N (398.9 eV, red). The additional weak satellite peak (dashed line) is assigned to shake-up processes. (b) Cobalt deposition gives rise to a fourth peak (399.9 eV, green) associated with Co-coordinated nitrogen. (c) The amount of *in situ* synthesized CoPyr is significantly increased by subsequent annealing (470 K during 5 h). (d) LEED pattern of (1 × 1)-reconstructed TiO_2(110) prior to any deposition. (e) 1 ML of Pyr exhibits a distinct superstructure which is observed over a wide coverage range and is not affected by the addition of Co (f).

an additional Co–N peak at 399.9 eV (green curve in Fig. 2) and the concomitant decrease of the pyridinic and iminic peak intensities as highlighted in Fig. 2b. A comparison of the peak areas allows to quantify the degree of metalation which amounts to 39 ± 10%. The metalation progresses further to 63 ± 10% upon annealing to 470 K (Fig. 2c). Variation of the ratio of deposited Co per Pyr molecule to 2 : 1 and 3 : 1 further increases the number of CoPyr complexes synthesized at room temperature (55 ± 10% and 75 ± 10%, respectively), and leads upon annealing to maximum metalation degrees of 73 ± 10% and 91 ± 10%, respectively. However, the excess supply of Co is expected to influence the electronic properties of the system and is avoided in the remainder of this work. Annealing at temperatures higher than 563 K leads to the irreversible decomposition of the molecules as indicated by changes in the N 1s spectrum (*cf.* Fig. S2 in ESI†).

Thus, the *in situ* metalation reaction of pyrphyrin by Co is found to be rather efficient on TiO_2. A similar study on the Ni metalation of tetraphenylporphyrin (TPP) on $TiO_2(110)$[31] reported initial metalation yields of 35 ± 5% and 60 ± 5% for Ni : TPP ratios of 1 : 1 and 3 : 1, respectively, which are close to our results. However, subsequent annealing to 550 K did not further increase the metalation yield of TPP. In the case of Pyr on Au(111) no direct Co-metalation was observed at room temperature.[13] This was assigned to clusters of Co formed upon deposition on the Pyr monolayer, as well as a prevalent Co-ligated intermediate state (CoPyr-2H) with two hydrogen atoms still present in the molecular core. Efficient incorporation of Co into the molecules required thermal energy to dissolve Co atoms from the observed clusters, for them to diffuse along the surface and to overcome an energy barrier for the metalation process from below.[13] The observation that Pyr on TiO_2 is readily metalated at room temperature might be attributed on the one hand to the stronger molecule–substrate interaction and the particular adsorption geometry of Pyr on $TiO_2(110)$. For example, the bent convex shape of Pyr on TiO_2 may facilitate the Co uptake. On the other hand the kinetics of the metalation reaction could be influenced by the diffusivity of Co on the substrate or a different propensity for Co cluster formation. Similarly, Ni metalation of TPP on reconstructed $TiO_2(110)$ (1 × 2) exhibits lower initial metalation yields than on $TiO_2(110)$ (1 × 1) due to lower diffusion rates on the more corrugated substrate.[32] However, subsequent annealing leads to higher final metalation yields which was attributed to the smaller size but higher density of Ni cluster on $TiO_2(110)$ (1 × 2).

In contrast to Pyr/Au(111) where several phases of molecular arrangements were observed as a function of pyrphyrin coverage and Co-metalation,[13] LEED patterns of Pyr/$TiO_2(110)$ show a single phase over a wide coverage range. The pattern in Fig. 2e suggests a distorted $c(8 \times 2)$ superstructure, while Fig. 2d gives the pattern from the clean (1 × 1)-reconstructed surface for reference. The Pyr-related superstructure spots simply get brighter and sharper with increasing coverage up to 1 ML, which indicates the formation of ordered domains in the sub-monolayer regime. Interestingly, the superstructure persists even after metalation with Co (Fig. 2f). This suggests a strong anchoring of the Pyr molecules in this particular adsorption geometry.

The experimental findings are corroborated by monolayer calculations of Pyr and CoPyr on $TiO_2(110)$ (*cf.* Fig. S12 and S13 in ESI†) which show that the adsorption structures of monomers and monolayers of both molecules are very similar and thus relatively independent of coverage and metalation. The adsorption energies are calculated as −3.76 eV and −3.73 eV for the Pyr and CoPyr monolayers, respectively. The molecule–substrate interactions are also very similar for the two cases: −5.26 eV for Pyr and −5.35 eV for CoPyr complexes. Relatively large values of the interaction energies are attributed to the substantial distortion of the monolayer structures on the $TiO_2(110)$ surface. Although there is repulsive interaction between the cyano nitrogen atoms of adjacent molecules, they still adsorb on the surface in a row direction similar to the monomer case. The smallest distance between two cyano nitrogen atoms of two Pyr (CoPyr) molecules becomes ≈3 Å with this adsorption configuration. In contrast, by relaxing the molecules in the gas phase, without the substrate, flat structures are obtained with ≈7 Å separated cyano nitrogen atoms. The contribution of the intermolecular interactions to the stability of the Pyr and the CoPyr monolayers are computed as −0.51 eV and −0.48 eV, respectively. Compared to the formation of disordered Co-phthalocyanine structures on $TiO_2(110)$,[33] our results suggest that the attractive molecule–substrate and intermolecular interactions together with the van der Waals interaction support the formation of ordered assemblies and sustain the stability of the monolayers on the oxide surface. See ESI† for the calculation of the energetic parameters and more details on the structural characteristics.

The molecular energy levels and their alignment relative to the substrate bands are addressed by UPS. Fig. 3a shows the normal emission survey spectra for 1 ML of Pyr (red), CoPyr (60% metalated; blue) and a Pyr multilayer for reference (dashed). Additionally, the spectrum of pristine $TiO_2(110)$ is given (shaded curve), showing the onset of the oxygen 2p band at a binding energy of 3.0 eV, in line with a recent study of the $TiO_2(110)$-(1 × 1) surface.[34] The gap region in Fig. 3c shows a weak feature centered at a binding energy of 0.9 eV which increases after metalation. It is most likely caused by a small amount of Ti 3d-related defects,[35] while a small contribution from minority Co(0) clusters cannot be excluded.

The spectrum of 1 ML Pyr/$TiO_2(110)$ (Fig. 3c) reveals molecular states within the TiO_2 bandgap. The shape of the peak indicates the presence of two states. By considering a quadratic tail of the valence band edge (red dashed curve), a deconvolution by two Voigt functions locates the HOMO and the HOMO−1 of Pyr/TiO_2 at binding energies of 2.14 ± 0.10 eV and 2.66 ± 0.10 eV, respectively. These states show no dispersion when the emission angle is scanned and they are thus localized on individual molecules. In the valence band region, it is difficult to disentangle further molecular states from the O 2p band of the substrate. Linear extrapolation of the valence band

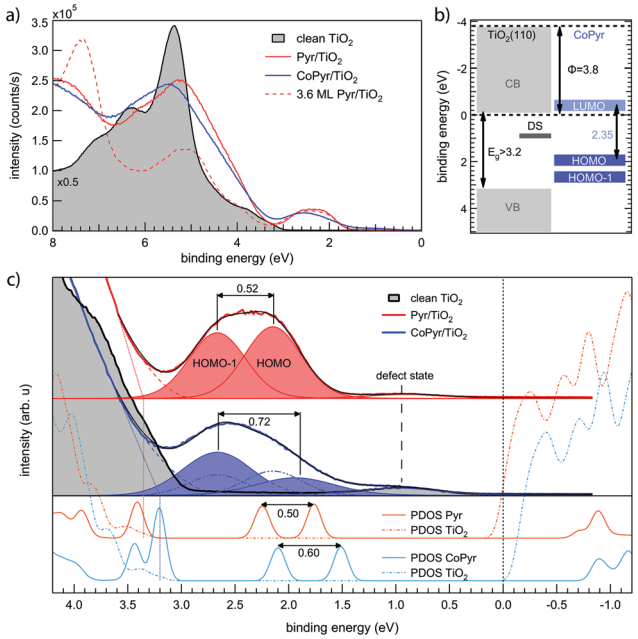

Fig. 3 (a) Normal emission UP-spectra of clean TiO_2(110) (black), with 1 ML Pyr (red) and CoPyr (blue, 60% metalated) in comparison to a Pyr multilayer (dashed). Molecular states appear within the bandgap of the substrate. (b) Energy scheme summarizing the key results of the CoPyr/TiO_2 system. The LUMO position is deduced from the measured position of the HOMO and the HOMO–LUMO gap of 2.35 eV obtained from our DFT calculations. (c) Bandgap region with arbitrary offsets added to the Pyr/TiO_2 spectrum. A deconvolution by Voigt functions locates the HOMO and HOMO–1 of Pyr/TiO_2 at 2.14 eV and 2.66 eV and of CoPyr/TiO_2 at 1.94 eV and 2.66 eV, respectively. The lower part of (c) shows the calculated DOS for Pyr (red) and CoPyr (blue) monolayers on TiO_2 projected to the respective molecules (solid lines) or to the substrate (dashed-dotted lines). The calculated spectra were broadened by a Gaussian function and aligned to the valence band onset of the corresponding experimental spectrum (vertical dotted lines).

edge (red dotted line in Fig. 3c) suggests a band bending change of 350 meV to higher binding energies due to Pyr adsorption (*cf.* Fig. S5 of ESI†). This general trend is confirmed by the calculated charge transfer from the Pyr and CoPyr molecules to the TiO_2 surface (*cf.* section 2.2.2 in ESI†). However, the apparent shift to higher binding energies is about 140 meV smaller after Co metalation (blue dotted line). Furthermore, the corresponding Ti $2p_{3/2}$ and O 1s core levels shift only slightly by in total less than 50 meV and unidirectionally to higher binding energies for Pyr adsorption and Co-incorporation. While we assigned this discrepancy to the higher surface sensitivity of UPS, it is nevertheless possible that the observed shifts in the UP-spectra are also affected by a changing background. With increasing Pyr coverage, the work function is observed to decrease significantly from Φ_{clean} = 4.9 ± 0.1 eV on clean TiO_2(110) to Φ_{Pyr} = 3.7 ± 0.1 eV at 0.75 ML Pyr coverage as illustrated in Fig. S6 of ESI.†

Cobalt incorporation does not induce a drastic variation of the measured UP-spectra (Fig. 3c). A slight overall broadening can be explained by the coexistence of CoPyr and Pyr in a ratio of 60 : 40 in this particular sample. As mentioned earlier, higher Co dosing was avoided in order to keep the surface free from metallic Co species. By taking the coexistence of Pyr and CoPyr into account, the spectrum was decomposed by four Voigt functions. The intensity ratio of the two Pyr related peaks as well as their binding energies and peak widths were fixed to their values obtained from the Pyr spectrum. The resulting fit yields CoPyr/TiO_2 HOMO and HOMO–1 binding energies of 1.94 ± 0.10 eV and 2.66 ± 0.10 eV, respectively. The molecular states remain dispersionless, and the work function does not change significantly (Φ_{CoPyr} = 3.8 ± 0.1 eV).

The aforementioned optimized monolayer adsorption geometries were used to calculate the density of states (DOS) of Pyr/TiO_2(110) and CoPyr/TiO_2(110) (*cf.* Fig. S14 in ESI† for total DOS spectra). The DOS projected on the molecules as well as on the substrates for the two complexes are represented in the lower part of Fig. 3c. The calculated spectra were aligned to the linear extrapolated valence band onset of the respective experimental spectrum. While this seems to be reasonable for CoPyr, in case of Pyr the calculated conduction band minimum appears directly at E_F due to the apparent shift of the measured valence band edge. Overall, we find that DFT predicts the relative distances between the HOMO and HOMO–1 of Pyr and CoPyr quite well, but fails to correctly align the molecular states with respect to the substrate bands. Fig. 3b summarizes the determined energy levels of CoPyr/TiO_2 (110). The LUMO at −0.41 eV is deduced by taking into account the measured HOMO energy of 1.94 eV and the calculated HOMO–LUMO gap of 2.35 eV. Due to the observed band bending, the conduction band is expected right above E_F. Thus, the present band alignment is indeed favorable for the absorption of visible light by the CoPyr molecules and subsequent injection of these excited electrons from the CoPyr LUMO to the conduction band of TiO_2(110).[11] The same holds also for Pyr/TiO_2(110) where the calculated HOMO–LUMO gap of 2.45 eV locates the LUMO at −0.31 eV.

Generally, the applicability of molecular dyes is strongly connected with their stability upon light irradiation. Continuous UV-irradiation of Pyr/TiO_2(110) is found to induce a rapid and monotonous decrease of the molecule related photoemission signals. Fig. 4a shows the evolution of the recorded spectra over time which indicate a photo-induced decomposition of the molecules. This is highlighted in Fig. 4c where the initial and final spectra of the time series are plotted. The temporal variations of intensities at selected energies I, II and III are illustrated in Fig. 4d (dashed lines). An approximately exponential behavior is observed with different decay constants for the three energies.

Metalation of the Pyr molecules changes this behavior dramatically. The incorporation of Co stabilizes the molecules and immunizes them against UV-induced degradation: Fig. 4b presents the temporal evolution of the UP-spectra after metalation. No spectral changes occur over the same time period during which significant degradation resulted in the

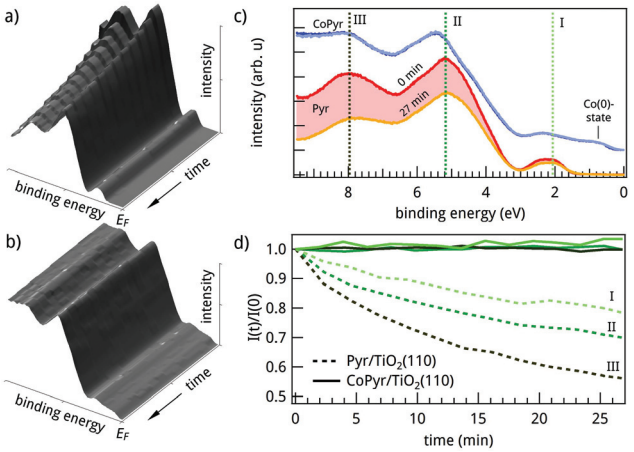

Fig. 4 Stability of (a) Pyr/TiO_2(110) and (b) CoPyr/TiO_2(110) under exposure to Helα radiation (21.2 eV), measured by continuously recording UP-spectra during 27 min. (c) Measured valence band spectra for Pyr and CoPyr with an arbitrary offset added to the latter. (d) Photoelectron yield as function of time at fixed binding energies I, II and III as marked in (c). Pyr (dashed lines) shows almost exponentially decaying states, whereas CoPyr (solid lines) appears to be stable over this time period.

Pyr/TiO_2(110) case. In order to produce a high percentage of metalated molecules, cobalt was supplied in a slightly over-stoichiometric amount in this preparation. As a consequence, approximately 0.08 ML of metallic Co is present on the surface. It can be identified as a Co(0) component in the Co 2p spectra (*cf.* Fig. S1 in ESI†) and produces an additional spectral feature around 0.9 eV which is visible in Fig. 4c. Please note, that a reference experiment showed the same UV-stability for *ex situ* prepared CoPyr deposited directly on TiO_2 (*cf.* Fig. S4 in ESI†). Thus, side reactions due to the metalation procedure can be excluded.

Our experimental and theoretical results for Pyr and CoPyr adsorbed on TiO_2(110) show that the molecular level scheme does not change dramatically upon metalation (Fig. 3c). We therefore argue that the increased stability of CoPyr is related to a dynamic effect. The fast degradation of the adsorbed Pyr molecules due to UV-irradiation could in principle have two different origins: direct photoexcitation of the molecule yields electronically excited states with potential energy surfaces that lead to dissociation. On the other hand, hot electrons resulting from photoexcitation of the TiO_2 substrate could fill unoccupied molecular states with strongly antibonding character, leading to the same result. The incorporation of a Co atom may enhance the electronic coupling to the substrate and/or induce additional degrees of freedom on the molecule, both electronic and vibrational. These effects would increase the number of de-excitation channels for electronically highly excited molecular states and consequently reduce the lifetimes of the excited states. Along these lines, we suspect three mechanisms to be mainly responsible for the increased photostability:

First, charge transfer from CoPyr towards the TiO_2 substrate could be facilitated due to an enhanced molecule–surface contact of the metalated molecule. The enhanced wave function overlap of the metalated molecule and the TiO_2 surface could reduce the lifetime of an excited state sufficiently to make bond dissociation less likely. However, our results provide only weak evidence for this scenario. The molecular levels of Pyr and CoPyr on TiO_2 differ only slightly. Moreover, geometry optimization results exhibit a very similar self-assembly behavior of both molecules on the surface with the CoPyr monolayer being minimally closer to the surface (0.03 Å) than the Pyr monolayer. Accordingly, the molecule–substrate interaction is slightly larger in the CoPyr case (*cf.* section 2.3 of ESI†).

Second, the readiness of the Co^{2+} ion for changing its charge state offers efficient channels for hot electrons from the substrate to dwell on the molecule without triggering decomposition. In fact, this is the same variability of the oxidation-state which renders CoPyr an efficient water reduction catalyst in solution.[8] According to previous studies, open d-shell metal complexes (*e.g.* Cu(II)-mesoporphyrin) reveal higher photostability than their closed shell equivalents (*e.g.* Zn(II)-mesoporphyrin) and bare ligands, respectively.[36] Calculations of the charge redistribution of neutral and negatively charged CoPyr molecules discussed in section 2.2.5 of ESI† support this potential buffer property of the Co ion. Charges of about +1.02*e* localize on the Co center for neutral CoPyr *in vacuo* and similarly for quasi-neutral CoPyr/TiO_2. The negatively charged CoPyr molecule *in vacuo* exhibits a charge of +0.71*e* at its Co center while the molecular orbitals are much less shifted than in the Pyr case.

Third, scattering between electrons and vibrational modes is another de-excitation channel which is capable of converting destructive electronic excitations into less harmful vibrational energy. This effect protects for example DNA from damage by UV-radiation.[37] N 1s spectra of unmetalated Pyr reveal that temperature-induced vibrational excitations up to 560 K only compromise the NH-bonds as shown in Fig. S2 in ESI.† In contrast, the UV-induced degradation seems to affect more than one nitrogen species of the bare ligand and thus reflects a more complex decomposition of the molecule (*cf.* Fig. S3 in ESI†). We suggest that the incorporation of the heavy metal ion introduces additional low frequency vibrational modes not present in the bare macrocycle.[38] In molecular crystals, it has been found that the coupling strength between such lower frequency modes and the electronic system scales inversely with the frequency squared.[39]

In addition, irreversible photodegradation of chlorophyll *a* (Chl*a*), Mg-TPP and other metal-porphyrins is known to be mainly a photo-oxidative process as O_2 interacts with the excited molecular state under illumination.[40,41] In the case of Chl*a*, Au nanoparticles were observed to have a photoprotective impact by binding to the nitrogen sites.[42] Whereas Co might play a comparable role in the stabilization of Pyr, this photo-oxidative process, however, may not account for the observed difference in photostability between CoPyr and Pyr, since we observe similar photodegradation of Pyr/Au(111), *i.e.*, in the absence of any reactive oxygen species.

4. Conclusions

The adsorption and metalation of pyrphyrin macrocycles on the stoichiometric TiO_2(110) surface has been investigated. STM images of adsorbed Pyr molecules taken at low coverage are consistent with the optimized adsorption geometry obtained from DFT calculations where molecules straddle the bridging oxygen rows in a convex fashion. At higher coverage, a well-defined molecular superstructure emerges with a distorted $c(8 \times 2)$ periodicity. Evaporation of Co leads to an efficient *in situ* metalation of Pyr/TiO_2(110) without influencing the molecular ordering. In agreement with our DFT-calculations, molecular states are found within the substrate bandgap for both, Pyr and CoPyr, with only minor energy shifts upon metalation. Continuous UV-irradiation induces rapid decomposition of the Pyr molecules, while Co-incorporation is found to stabilize the molecules against photo-induced degradation. This strongly enhanced stability of CoPyr is of particular importance for its potential use in dye sensitization of TiO_2.

Acknowledgements

This project has been financed under the University Research Priority Program LightChEC of the University of Zurich, the FP7 Marie Curie COFUND scheme of the European Commission, and the National Centres of Competence in Research–Materials Revolution: Computational Design and Discovery of Novel Materials (NCCR–MARVEL). We acknowledge computing resources from the Swiss National Supercomputer Centre (CSCS) under the project ID s425 and expert technical support by Thomas Kälin.

References

1 B. A. Pinaud, J. D. Benck, L. C. Seitz, A. J. Forman, Z. B. Chen, T. G. Deutsch, B. D. James, K. N. Baum, G. N. Baum, S. Ardo, H. L. Wang, E. Miller and T. F. Jaramillo, *Energy Environ. Sci.*, 2013, **6**, 1983–2002.
2 A. Fujishima and K. Honda, *Nature*, 1972, **238**, 37–38.
3 T. Jafari, E. Moharreri, A. S. Amin, R. Miao, W. Song and S. L. Suib, *Molecules*, 2016, **21**, 900.
4 A. Fujishima, X. Zhang and D. A. Tryk, *Surf. Sci. Rep.*, 2008, **63**, 515–582.
5 M. A. Henderson, *Surf. Sci. Rep.*, 2011, **66**, 185–297.
6 M. Wang, Y. Na, M. Gorlov and L. Sun, *Dalton Trans.*, 2009, 6458–6467.
7 S. Losse, J. G. Vos and S. Rau, *Coord. Chem. Rev.*, 2010, **254**, 2492–2504.
8 E. Joliat, S. Schnidrig, B. Probst, C. Bachmann, B. Spingler, K. K. Baldridge, F. von Rohr, A. Schilling and R. Alberto, *Dalton Trans.*, 2016, **45**, 1737–1745.
9 S. Ogawa, R. Narushima and Y. Arai, *J. Am. Chem. Soc.*, 1984, **106**, 5760–5762.
10 F. Li, K. Fan, B. Xu, E. Gabrielsson, Q. Daniel, L. Li and L. Sun, *J. Am. Chem. Soc.*, 2015, **137**, 9153–9159.
11 Y. Gurdal, S. Luber, J. Hutter and M. Iannuzzi, *Phys. Chem. Chem. Phys.*, 2015, **17**, 22846–22854.
12 J. M. Gottfried, *Surf. Sci. Rep.*, 2015, **70**, 259–379.
13 G. Mette, D. Sutter, Y. Gurdal, S. Schnidrig, B. Probst, M. Iannuzzi, J. Hutter, R. Alberto and J. Osterwalder, *Nanoscale*, 2016, **8**, 7958–7968.
14 T. Greber, O. Raetzo, T. Kreutz, P. Schwaller, W. Deichmann, E. Wetli and J. Osterwalder, *Rev. Sci. Instrum.*, 1997, **68**, 4549–4554.
15 U. Diebold and T. Madey, *Surf. Sci. Spectra*, 1998, **4**, 227–231.
16 J. VandeVondele, M. Krack, F. Mohamed, M. Parrinello, T. Chassaing and J. Hutter, *Comput. Phys. Commun.*, 2005, **167**, 103–128.
17 S. Goedecker, M. Teter and J. Hutter, *Phys. Rev. B: Condens. Matter*, 1996, **54**, 1703–1710.
18 J. VandeVondele and J. Hutter, *J. Chem. Phys.*, 2007, **127**, 114105.
19 J. P. Perdew, K. Burke and M. Ernzerhof, *Phys. Rev. Lett.*, 1996, **77**, 3865–3868.
20 S. Grimme, J. Antony, S. Ehrlich and H. Krieg, *J. Chem. Phys.*, 2010, **132**, 154104.
21 J. Heyd, G. E. Scuseria and M. Ernzerhof, *J. Chem. Phys.*, 2003, **118**, 8207–8215.
22 A. V. Krukau, O. A. Vydrov, A. F. Izmaylov and G. E. Scuseria, *J. Chem. Phys.*, 2006, **125**, 224106.
23 T. L. Bahers, M. Rérat and P. Sautet, *J. Phys. Chem. C*, 2014, **118**, 5997–6008.
24 L.-H. Han, C.-R. Zhang, J.-W. Zhe, N.-Z. Jin, Y.-L. Shen, W. Wang, J.-J. Gong, Y.-H. Chen and Z.-J. Liu, *Int. J. Mol. Sci.*, 2013, **14**, 20171–20188.
25 M. Guidon, J. Hutter and J. VandeVondele, *J. Chem. Theory Comput.*, 2010, **6**, 2348–2364.
26 M. Guidon, J. Hutter and J. VandeVondele, *J. Chem. Theory Comput.*, 2009, **5**, 3010–3021.
27 M. Guidon, F. Schiffmann, J. Hutter and J. VandeVondele, *J. Chem. Phys.*, 2008, **128**, 214104.
28 P. Rahe, R. Bechstein and A. Kühnle, *J. Vac. Sci. Technol., B*, 2010, **28**, C4E31–C4E38.
29 U. Diebold, J. Lehman, T. Mahmoud, M. Kuhn, G. Leonardelli, W. Hebenstreit, M. Schmid and P. Varga, *Surf. Sci.*, 1998, **411**, 137–153.
30 L. Ottaviano, L. Lozzi, F. Ramondo, P. Picozzi and S. Santucci, *J. Electron Spectrosc. Relat. Phenom.*, 1999, **105**, 145–154.
31 C. Wang, Q. Fan, S. Hu, H. Ju, X. Feng, Y. Han, H. Pan, J. Zhu and J. M. Gottfried, *Chem. Commun.*, 2014, **50**, 8291–8294.
32 C. Wang, Q. Fan, Y. Han, J. I. Martinez, J. A. Martin-Gago, W. Wang, H. Ju, J. M. Gottfried and J. Zhu, *Nanoscale*, 2016, **8**, 1123–1132.

33 N. Ishida and D. Fujita, *J. Phys. Chem. C*, 2012, **116**, 20300–20305.
34 A. Borodin and M. Reichling, *Phys. Chem. Chem. Phys.*, 2011, **13**, 15442–15447.
35 K. Mitsuhara, H. Okumura, A. Visikovskiy, M. Takizawa and Y. Kido, *J. Chem. Phys.*, 2012, **136**, 124707.
36 J. B. Zvezdanović, D. Z. Marković and S. M. Milenković, *J. Serb. Chem. Soc.*, 2012, **77**, 187–199.
37 H. Satzger, D. Townsend, M. Z. Zgierski, S. Patchkovskii, S. Ullrich and A. Stolow, *Proc. Natl. Acad. Sci. U. S. A.*, 2006, **103**, 10196–10201.
38 J. Kincaid and K. Nakamoto, *J. Inorg. Nucl. Chem.*, 1975, **37**, 85–89.
39 A. Devos and M. Lannoo, *Phys. Rev. B: Condens. Matter*, 1998, **58**, 8236–8239.
40 J. Zhang, P. Zhang, Z. Zhang and X. Wei, *J. Phys. Chem. A*, 2009, **113**, 5367–5374.
41 J. B. Zhang, P. Y. Zhang, G. H. Chen, F. Han and X. H. Wei, *Chin. Chem. Lett.*, 2008, **19**, 1190–1192.
42 S. Barazzouk, L. Bekalé and S. Hotchandani, *J. Mater. Chem.*, 2012, **22**, 25316–25324.